frontiers | Frontiers in Physics

TYPE Original Research
PUBLISHED 04 October 2022
DOI 10.3389/fphy.2022.996001



OPEN ACCESS

EDITED BY
Breno R. L. Galvão,
Federal Center for Technological Education of Minas Gerais, Brazil

REVIEWED BY
Oleg Polyansky,
University College London, United Kingdom
Joseph Abebe Obu,
University of Calabar, Nigeria

*CORRESPONDENCE
János Sarka,
Janos.Sarka@ttu.edu

SPECIALTY SECTION
This article was submitted to Physical Chemistry and Chemical Physics, a section of the journal Frontiers in Physics

RECEIVED 16 July 2022
ACCEPTED 12 August 2022
PUBLISHED 04 October 2022

CITATION
Sarka J and Poirier B (2022), Assigning quantum labels and improving accuracy for the ro-vibrational eigenstates of $H_3^+$ calculated using ScalIT. *Front. Phys.* 10:996001. doi: 10.3389/fphy.2022.996001



# Assigning quantum labels and improving accuracy for the ro-vibrational eigenstates of $H_3^+$ calculated using *ScalIT*

János Sarka* and Bill Poirier

Department of Chemistry and Biochemistry, Texas Tech University, Lubbock, TX, United States

In a recent article [AIP Adv. 11, 045033 (2021)], we carried out exact quantum dynamical calculations and computed ro-vibrational energy levels and wave functions for the $H_3^+$ molecular ion up to the dissociation threshold (at $J = 46$) using a recently developed potential energy surface (PES) [Mol. Phys. 117, 1663 (2019)]—arguably, the most accurate to date —together with the ***ScalIT*** suite of parallel codes. In this work, we further improved the convergence accuracy and range of our ***ScalIT*** calculations for all $J$ values up to $J = 20$ to a few $10^{-5}$ cm$^{-1}$ (or better). In addition, we performed an *ab initio* assignment of the ro-vibrational energy levels, providing vibrational '$v_1$, $v_2$, $|l|$' and rotational '$J$, $G$, $U$, $K$' quantum labels for more than 2,200 ro-vibrational states, including every single $0 \le J \le 20$ state up to and above the barrier to linearity at 10,000 cm$^{-1}$. The main underlying motivation of our work is to provide a list of reliably labeled, spectroscopically accurate energy levels in a format that can be used in spectroscopic line lists, which are based on both experimental and theoretical levels. Such line lists are of huge importance in various astrochemical and astrophysical contexts.

KEYWORDS

**ab initio, ro-vibrational energy levels, quantum label assignment, high accuracy, ScalIT code**

## 1 Introduction

The $H_3^+$ molecular ion [1]—the smallest tri-atomic molecular system, with just three protons and two electrons—is a central molecule in molecular astrophysics and astrochemistry. It is the most common molecular ion in the Universe, serving as the main conduit of chemical reactions in outer space. $H_3^+$ can be found in the interstellar medium [2], supernova remnants [3], the atmospheres of gas giants, and exoplanets [4, 5], and also plays an important role in star formation [1]. Partially due to its simplicity, $H_3^+$ serves as a benchmark system for several different areas of science, in particular, high-resolution ro-vibrational spectroscopy experiments, accurate *ab initio* electronic structure calculations and potential energy surface (PES) development, high performance quantum dynamics calculations, and reaction dynamics. Despite its simplicity, the near-dissociation spectrum of $H_3^+$ [6, 7]—recorded 40 years ago!—still remains unassigned.

$H_3^+$ has been studied very extensively both experimentally and computationally in the last four decades, as was recently summarized in a very nice review [1].

On the experimental side, numerous spectroscopic studies have been conducted [6–14]. Of course, the primary challenge with respect to labeling is that experiments provide only spectroscopic *transitions*, not the ro-vibrational energy levels themselves. Although symmetry and selection rules help, extracting the latter from the former remains a challenge, and has traditionally been something of a "black art." Recently, more systematic approaches have been developed, based on graph theory and "spectroscopic networks" (SNs) [15, 16], in which the vertices represent rovibrational energy levels, and the lines represent experimentally observed spectroscopic transitions, to extract empirical energy levels directly from experimental data, with well-defined and realistic uncertainties. In particular, the MARVEL code (Measured Active Rotational–Vibrational Energy Levels) [17, 18], has been applied to ro-vibrational spectroscopic data of $H_3^+$ that were collected from 26 separate experimental sources [13]. The resultant energy levels and assignments replaced the earlier work of [8]. A MARVEL analysis was also carried out for two isotopologues, $H_2D^+$ and $D_2H^+$ [14], with the database last updated in 2019 [19]. Thus far, the number of validated, and therefore recommended, experimental quality ro-vibrational energy levels of $H_3^+$ are 652, [19] of which 259 belong to ortho-$H_3^+$ ($I$ = 3/2) and 393 to para-$H_3^+$ ($I$ = 1/2), with $I$ being the quantum number of the total nuclear spin of the system.

On the theoretical side, due to its spectroscopic importance, a variety of $H_3^+$ PESs have been developed over the years [11, 12–26]—with the latest two [25, 26] published only very recently. A number of ro-vibrational state calculations have also been performed in the past for this system [12, 22–43], many employing empirical corrections of various kinds (e.g., empirically modified vibrational masses [44, 45]) in order to better match the available experimental data, and also to capture non-adiabatic effects [24, 25, 34, 37–39, and 41]. The empirical approach might be less effective at higher energies, [35]—e.g., in the context of reactive collisions, which have also been extensively studied for $H_3^+$ [46–48]. Additionally, empirical "corrections" can become a bit tricky, if there is any question as to how to match experimental and theoretical state labels.

For these reasons, we prefer a fully *ab initio* computational approach [43], both with regard to the ro-vibrational state calculation itself, as well as the determination of state labels. In particular, to the best of our knowledge, we are the first group to attempt a fully *ab initio* assignment of ro-vibrational state labels for $H_3^+$. Our first push in this direction was published in an article last year [43]; however, the set of $J$ values considered in that work was restricted, and in addition, we did not use wave functions to help determine ro-vibrational state labels, but only $D_{3h}$ symmetry labels. In addition, although the calculations were very well converged ($10^{-4}$ cm$^{-1}$), better convergence would have allowed for a better determination of symmetry-induced vs. "accidental" degeneracies, which in turn leads to a less ambiguous state labeling, especially at higher vibrational and rotational excitation energies. All of these small deficiencies of the previous work have been rectified here, as discussed below.

As further motivation for adopting a purely *ab initio* approach, we point out that $H_3^+$ has always been targeted as an important benchmark system for achieving a direct spectroscopic agreement between theory and experiment. This has been a long-standing goal, which it can be argued, has only begun to be obtained fairly recently [12, 24]. Additionally, the highly accurate determination of the ro-vibrational spectrum of astrophysically relevant molecules such as $H_3^+$ is motivated by the "weed problem" [49, 50]. In the interstellar medium and planetary atmospheres, many different molecules or ions are present at the same time. As the spectra overlap, it is crucial to obtain highly accurate spectra in order to unambiguously differentiate the contributions from different species.

Therefore, creating highly accurate line lists can serve as an important tool, from both the experimental and computational points of view. The first such line list was created by [51] with 669 astronomically important lines. This was supplemented by [52], with about three million lines. The newest line list, MiZaTeP [53], contains more than 120 million lines by bringing together the experimental spectroscopic data using MARVEL [13], and theoretical levels computed with the DVR3D code [54–56]. This line list also contains 17 meta-stable states, which are quantum states with very long lifetimes.

In this work, in order to facilitate the expansion of already existing $H_3^+$ line lists, we focus our efforts on further improving the convergence accuracy of our *ab initio* ro-vibrational energy level calculations down to a few $10^{-5}$ cm$^{-1}$. This is far beyond the accuracy of the PES, and certainly much smaller than the discrepancies within the experiment. Nevertheless, such an extraordinarily high convergence accuracy is essential with respect to unambiguous state labeling, as discussed, especially at higher vibrational and rotational excitation energies. Additionally, we compute and analyze ro-vibrational wave functions to determine their "vibrational parent" states [57] as a further means of providing unambiguous labels. In the present work, we also consider *all* values of the rotational quantum number $J$, not just selected values—but only up to a maximum of $J$ = 20. In the previous work [43], we considered higher $J$ values, all the way up to rotational dissociation ($J$ = 46). Here, we apply a restriction to comparatively low values, simply because the quantum label assignment (which is a primary focus of this work) becomes essentially impossible much beyond this point.

In all, we provide vibrational '$v_1$, $v_2$, $|l|$' and rotational '$J$, $G$, $K$, $U$' quantum labels for more than 2,200 ro-vibrational states, around 1,600 of which are new assignments complementing, and in certain cases arguably correcting, the ~650 assignments in the MARVEL database [19]. To the best of our knowledge, no previous work has attempted to provide purely *ab initio* quantum label assignments for computed ro-vibrational states—certainly not to the extent that we have done here, in any event.

## 2 Materials and methods

In a recent article [43], we carried out the exact ro-vibrational energy level and wave function calculations for the $H_3^+$ molecular ion for selected $J$ values up to $J$ = 46. As most of the computational details remain unchanged, here, we only provide a brief summary of the overall computational methodology, and focus primarily on the differences from the previous work.

### 2.1 *ScalIT*

The quantum dynamical calculations presented in this article were performed using the ***ScalIT*** [58–62] suite of parallel codes. ***ScalIT*** is a black-box molecular ro-vibrational spectroscopy code, which for tri- and tetratomic molecules employs an analytical kinetic energy operator expressed in (orthogonal) Jacobi coordinates. The use of direct product basis sets (DPBs) including discrete variable representations (DVRs) results in a Hamiltonian matrix with a sparse structure. For the radial coordinates, phase–space-optimized DVRs (PSO-DVRs) are used [63–68] while for the bend and rotation angles, standard associated Legendre polynomial or Wigner rotation function basis sets are utilized. The Hamiltonian is diagonalized iteratively using sparse Krylov subspace methods together with several different effective numerical optimization strategies, such as the preconditioned inexact spectral transform (PIST) method [69–71], optimal separable basis (OSB) preconditioning [72–75], and the standard iterative quasi-minimal residual (QMR) algorithm [59, 76]. All of these methods working together ensure the effective scaling across massively parallel supercomputing clusters (up to a few thousand cores) and the ability of ***ScalIT*** to accurately compute even extremely energetically high-lying quantum states. So far, ***ScalIT*** has been used for around a dozen challenging systems, such as $Ne_4$ and HCCH [43, 50, 68, and 77–86], and via extending the capabilities of the ***ScalIT*** code through the ***SwitchIT*** [87] algorithm to accommodate more complicated Hamiltonians, even $CH_3CN$ [87].

The massively parallel capability of ***ScalIT*** is based on MPI parallelization, which makes the code uniquely qualified to compute many quantum states with high accuracy for small molecular systems. Other available ro-vibrational spectroscopy codes, e.g., ***DVR3D*** [54–56], ***TROVE*** [88–90], ***DOPI*** [33, 91, 92], ***DEWE*** [57, 93–95], ***GENIUSH*** [96, 97], and ***ElVibRot*** [98–100], in general traditionally only offer single node OPENMP parallelization (although ***ElVibRot*** has been made MPI parallel recently [101]). Also, it is worth mentioning that the use of GPUs is spreading slowly to the field of ro-vibrational molecular spectroscopy with a focus on computing ro-vibrational intensities [102].

### 2.2 Potential energy surface

In this work, we utilized the recently computed $H_3^+$ PES referred to as "PES75K+" [25] which is based on the Born–Oppenheimer *ab initio* points of the earlier "GLH3P″ PES [12, 24], the first "calibration quality" PES developed for $H_3^+$. In our previous work, we compared these two PESs and discussed the spurious asymptotic wells that appear in the GLH3P PES [43], which were causing significant numerical convergence problems for our ***ScalIT*** calculations. Although GLH3P has been used more frequently in previous computational ro-vibrational spectroscopy studies, PES75K+ has now been shown to provide more accurate energy levels higher up in the spectrum.

In any event, the $H_3^+$ PES shows this molecular ion to be quite stable. The first dissociation threshold (to $H_2 + H^+$) occurs at $D_0 = 35,076 \pm 2$ cm$^{-1}$ [25]. However, there is a much lower-lying (linear) isomerization barrier at around 10,000 cm$^{-1}$.

### 2.3 Previous computational works

For the GLH3P PES [12, 24]—and other earlier PESs, including the PES developed by Cencek and colleagues [20, 21]—a wide range of ro-vibrational calculations have been performed [12, 22–24, 27–29, 31, 32, 34–40, 42, and 43]. Most of these are summarized in a fairly recent review article [40]. In the last couple of years, newer PESs have been also developed, among them, the PES75K+ PES [25] is used here, and also a multi-sheet fit PES including more than one electronic state [26]. By and large, the ro-vibrational studies have focused on increasing the accuracy of numerical convergence, as well as pushing the limits of vibrational/rotational excitation. Indeed, computing ro-vibrational energy levels of $H_3^+$ near dissociation has a long history [3, 27, 29]. To date, all energy levels were computed up to dissociation using atomic [30, 33], nuclear [35], and modified hydrogen masses [35] to investigate the properties of high-lying vibrational states. More restricted calculations—both in terms of energy and rotational

excitation, but also accuracy—were also carried out, up to $J$ = 2 and 15,300 $cm^{-1}$ [32], and up to $J$ = 3 and the then-experimental limit of ~17,000 $cm^{-1}$ [24]. The dependence of Coriolis coupling on choice of "embedding" or body-fixed frame was also investigated [42].

## 2.4 Symmetry

Jacobi coordinates (denoted as $r$, $R$, and $\theta$ here) are usually the best choice for describing $AB_2$ triatomic molecules. In such cases, the full $G_4$ permutation–inversion (PI) symmetry of the molecules is fully described. Of course, $H_3^+$, with its three identical atomic nuclei, is an $A_3$ system, whose energy levels are labeled by the $G_{12}$ PI group irreducible representations (irreps) [103]. Note that $G_{12}$ is isomorphic with the $D_{3h}$ point group—which, in any event, describes the global minimum equilibrium structure of $H_3^+$, which is an equilateral triangle with a bond length of $1.65034a_0$ = 0.873 322Å.

Nevertheless, since Jacobi coordinates, in contrast to hyperspherical coordinates [104], do not respect the cyclic permutation operations of the $G_{12}$ PI group, this poses certain challenges for the ***ScalIT*** calculation performed here, which essentially presumes an $AB_2$ structure. More specifically, it becomes necessary to correlate the symmetry labels from the $G_4$ symmetry-adapted ***ScalIT*** calculations to the $G_{12}/D_{3h}$ labels, using the $\Gamma(D_{3h}) \downarrow G_4$ correlation table [43]. The "challenge" here actually only concerns the doubly-degenerate $D_{3h}$ irrep pairs, which are computed in different ***ScalIT*** calculations corresponding to different $G_4$ irreps. In practice, one looks for identical eigenvalues across two $G_4$ irreps, and identifies those as comprising, in reality, a single doubly-degenerate $G_{12}$ irrep pair. Better convergence accuracy thus greatly improves the determination of numerically "identical" eigenvalues. Conversely, whatever pair splitting is observed numerically may be taken as an additional, independent measure of the overall numerical convergence accuracy.

The solutions of the $AB_2$ Jacobi Hamiltonian are computed in four separate "symmetry blocks", corresponding to the four (singly-degenerate) irreps of $G_4$. These irreps can be labeled by two good quantum numbers, $p$ = ±1 (associated with the exchange of any two identical nuclei) and $\epsilon$ = ±1 (the total parity). In addition, there are the two good rotational quantum numbers that can be used as completely reliable labels—i.e., the total angular momentum, $J$, and its projection along the space-fixed $Z$ axis, $M$. The third rotational quantum number, $K$, associated with the projection of $\hat{\vec{J}}$ along the *body-fixed z* axis, is technically not a good quantum number—though for $H_3^+$, it may still often be used as a state label in practice, together with other approximate labels described in Section 3.2.

Lastly, given the fermionic nature of the H atom nuclei (i.e., protons), it is worth mentioning that the Pauli principle requires the total spin-plus-spatial nuclear wave function to have a totally anti-symmetric or $A_2$ character (in the $S_3$ permutation subgroup of the $G_{12}$ PI group). For three such particles, the eight-dimensional combined nuclear spin space representation reduces to an irrep direct sum as $4A_1 \oplus 2E$. The corresponding spatial wave functions (i.e., the ro-vibrational states actually computed) are thus restricted to belonging to either the $A_2$ or E irreps. Therefore, all $A_1$ ro-vibrational states (including what would otherwise be the ground vibrational state), are unphysical, and must be ignored.

TABLE 1 The total bend-rotation angular basis sizes of each $G_4$ symmetry block, $N_{jK}^{A^+}$, $N_{jK}^{B^+}$, $N_{jK}^{A^-}$, and $N_{jK}^{B^-}$, for all *ScalIT* calculations of $H_3^+$ performed here, from total angular momentum $J$ = 0 to $J$ = 20. The number of bend-angle basis functions in $\theta$, i.e., $j_{max}$, is always equal to 36. The radial basis sizes are $N_r = N_R$ = 300, and the radial ranges (in atomic units) are $r_{min}$ = 0.5, $R_{min}$ = 0.0, and $r_{max} = R_{max}$ = 5.0.

| | $G_1$ | $G_2$ ($S_2$) blocks | | $G_4$ blocks | | | |
|---|---|---|---|---|---|---|---|
| $J$ | $N_{jK}$ | $N_{jK}^{A}$ | $N_{jK}^{B}$ | $N_{jK}^{A^+}$ | $N_{jK}^{B^+}$ | $N_{jK}^{A^-}$ | $N_{jK}^{B^-}$ |
| 0 | 37 | 37 | 0 | 19 | 18 | 0 | 0 |
| 1 | 109 | 36 | 73 | 18 | 18 | 37 | 36 |
| 2 | 179 | 108 | 71 | 55 | 53 | 36 | 35 |
| 3 | 247 | 105 | 142 | 53 | 52 | 72 | 70 |
| 4 | 313 | 175 | 138 | 89 | 86 | 70 | 68 |
| 5 | 377 | 170 | 207 | 86 | 84 | 105 | 102 |
| 6 | 439 | 238 | 201 | 121 | 117 | 102 | 99 |
| 7 | 499 | 231 | 268 | 117 | 114 | 136 | 132 |
| 8 | 557 | 297 | 260 | 151 | 146 | 132 | 128 |
| 9 | 613 | 288 | 325 | 146 | 142 | 165 | 160 |
| 10 | 667 | 352 | 315 | 179 | 173 | 160 | 155 |
| 11 | 719 | 341 | 378 | 173 | 168 | 192 | 186 |
| 12 | 769 | 403 | 366 | 205 | 198 | 186 | 180 |
| 13 | 817 | 390 | 427 | 198 | 192 | 217 | 210 |
| 14 | 863 | 450 | 413 | 229 | 221 | 210 | 203 |
| 15 | 907 | 435 | 472 | 221 | 214 | 240 | 232 |
| 16 | 949 | 493 | 456 | 251 | 242 | 232 | 224 |
| 17 | 989 | 476 | 513 | 242 | 234 | 261 | 252 |
| 18 | 1027 | 532 | 495 | 271 | 261 | 252 | 243 |
| 19 | 1063 | 513 | 550 | 261 | 252 | 280 | 270 |
| 20 | 1097 | 567 | 530 | 289 | 278 | 270 | 260 |

# 3 Results

## 3.1 Computational details

***ScalIT*** computations were carried out using nuclear masses, just as in our previous article [43]. The computational parameters of this work are summarized in Table 1. In DVR

calculations such as those performed here, very often as one increases the basis size in order to improve numerical convergence, one crosses over from a regime where the basis set truncation error dominates, to a regime where the numerical quadrature error dominates. This is indicated by a fast, variational convergence (from above) being replaced by a slow, oscillatory convergence behavior. Usually, when this crossover has occurred, it becomes computationally unfeasible to push the calculation much further through a "brute force" increase in the basis size.

For extremely accurately converged ro-vibrational calculations, it is therefore necessary to ensure that the quadrature error is minimized. This requires two conditions. First, the PES must be very smooth and well-behaved—which, in the case of PES75K+ (but unlike GLH3P), has already been established. Second, the "primitive basis" calculations used to compute the PSO DVR basis representations must be performed as accurately as possible. To this end, a very large number of 1,001 primitive sinc-DVR grid points were used in the PSO DVR calculations for both of the Jacobi radial coordinates, $r$ and $R$. The radial ranges used here were also wider than before [43]; here, we used $r_{\min} = 0.5$ bohr, and $r_{\max} = 5.0$ bohr for the $r$ coordinate, and $R_{\min} = 0.0$ bohr, and $R_{\max} = 5.0$ bohr for the $R$ coordinate.

Having put these measures into effect, our next task was to increase the basis sizes for the final calculation as far as possible, in hopes that an extremely high numerical convergence could be achieved prior to crossing over into the quadrature-error-dominated regime. We therefore used significantly larger radial basis sizes than in the previous calculation; i.e., $N_r = 300$ and $N_R = 300$. The angular dimensions were also increased compared to our previous work [43]; specifically, the number of bend-angle basis functions in the Jacobi coordinate $\theta$ was set to $j_{\max} = 36$ for every $J$ value considered. The resultant total bend-rotation angular basis sizes for each $G_4$ symmetry block calculation, i.e., $N_{jK}^{A^+}$, $N_{jK}^{B^+}$, $N_{jK}^{A^-}$, and $N_{jK}^{B^-}$, are listed in Table 1. Using these parameters, we were able to achieve better than $10^{-5}$ cm$^{-1}$ numerical convergence for all ro-vibrational states with $J \leq 10$.

## 3.2 State Labeling

The ro-vibrational calculations of $H_3^+$ for each $J > 0$ were carried out in four blocks corresponding to the four $G_4$ irreps. Note that the inversion parity is linked to the value of $K$, with even $\epsilon = +1$ parity corresponding to the even $K$ values, and odd $\epsilon = -1$ parity to the odd $K$ values. Thus, for $J = 0$, we only have two even parity blocks. States with $|K| \bmod 3 = 0$ are ortho-states with a spin weighting $g_s = 4$, while those with $K$ not exactly divisible by 3 are para-states with $g_s = 2$ [1]. As the convergence accuracy of our calculations is very high, the degenerate energy levels can be unambiguously identified, and therefore, it is easy to assign the $D_{3h}$ (i.e., $G_{12}$) irrep labels even for highly vibrationally and rotationally excited states.

Next, we address the vibrational state labels. The $H_3^+$ molecular ion has two normal modes, the totally symmetric stretch mode $\nu_1$ (belonging to the singly degenerate $A_1$ irrep), and the asymmetric stretch-bend mode, $\nu_2$ (belonging to the doubly degenerate $E$ irrep). Displacements of the latter distort the $A_1$ symmetry of the global minimum geometry, thereby producing a transition dipole moment. Also, being doubly degenerate, excitations of the $\nu_2$ mode give rise to a new quantum number, the vibrational angular momentum $l$, adopting the values, $l = \{\nu_2, \nu_2 - 2, \ldots - \nu_2 + 2, -\nu_2\}$. Therefore, the vibrational part of the ro-vibrational states can be described by the labels, '$\nu_1$, $\nu_2$, $|l|$'—although it must be borne in mind that these quantum numbers are not perfectly "good". Also note that the quantum number $|l|$ is linked to the $D_{3h}$ irrep labels. In particular, the $l = 0$ vibrational states are always singly degenerate $A_1'$ states. For $|l| > 0$, the degenerate pair can be labeled as $E'$, unless $|l| \bmod 3 = 0$, for which the $\pm l$ pair splits into an $A_1'$ and an $A_2'$ state.

After first determining the $D_{3h}$ irrep labels, we assigned vibrational state labels to the $J = 0$ pure-vibrational states, which were found to be in complete agreement with earlier studies [9, 10, 12, 13, 24, 32, and 43]. For $J > 0$, it is advantageous to first determine the vibrational labels, indicating which "vibrational parent" state the ro-vibrational state "belongs to". This is straightforward to do for low-vibrational and/or rotational excitations, where the energy level spacing is so high that the rotational progressions do not overlap. Higher up in energy, determining the "vibrational parents" becomes much more challenging. For $J = 1$, the different ro-vibrational progressions start to overlap at the 26th vibration at 10,000 cm$^{-1}$. Increasing $J$, this threshold energy value shifts down drastically. For $J = 11$, even the ro-vibrational states belonging to the zero-point vibration start to overlap with the ro-vibrational progression of the first vibration. Beyond a certain point in both ($\nu_1$, $\nu_2$, $|l|$) and $J$, it becomes impossible to assign vibrational parents based solely on energy values and $D_{3h}$ symmetry labels.

In order to overcome this difficulty, the ***GENIUSH*** code [96, 97] was invoked, which is capable of semi-automatically assigning vibrational parent labels using the rigid rotor decomposition scheme (RRD) [57], based on computing wave function overlaps. To do this, the ***ScalIT*** calculations were repeated using ***GENIUSH***, but with greatly reduced accuracy ($10^{-2}$–$10^{-3}$ cm$^{-1}$)—which was nevertheless sufficient to match the energy levels with the ***ScalIT*** ones. The RRD overlap matrices were then computed using ***GENIUSH***. In this manner, we were able to assign vibrational parent labels to much more highly excited ro-vibrational states—and for many more such states—than was previously possible.

We next move on to rotational state labels. The $H_3^+$ molecular ion can be characterized as an oblate symmetric top, for which

TABLE 2 The lowest ro-vibrational energy levels of $H_3^+$, in $cm^{-1}$, up to $J = 20$ total angular momentum and their comparison with the literature. The past calculations employed different PESs and masses (VRM stands for Unequal Vibrational and Rotational Masses) [35].

| | PES75K+ | | GLH3P PES | | | Comparison | | | |
|---|---|---|---|---|---|---|---|---|---|
| | nuclear mass | | | | VRM | | | | |
| *J* | This work | Ref. 43 | Ref. 43 | Ref. 35 | Ref. 35 | Ref. 43 | Ref. 43 | Ref. 35 | Ref. 35 |
| 0 | 0.0000 | 0.0000 | 0.0000 | 0.0000 | 0.0000 | 0.0000 | 0.0000 | 0.0000 | 0.0000 |
| 1 | 64.1277 | 64.1273 | 64.1283 | 64.1283 | 64.1233 | 0.0004 | −0.0006 | −0.0006 | 0.0044 |
| 2 | 169.3071 | 169.3075 | 169.3086 | 169.3086 | 169.2872 | −0.0004 | −0.0015 | −0.0015 | 0.0199 |
| 3 | 315.3617 | 315.3621 | 315.3644 | 315.3644 | 315.3164 | −0.0004 | −0.0027 | −0.0027 | 0.0453 |
| 4 | 502.0545 | 502.0549 | 502.0588 | 502.0588 | 501.9737 | −0.0004 | −0.0043 | −0.0043 | 0.0808 |
| 5 | 729.0368 | 729.0372 | 729.0431 | 729.0431 | 728.9106 | −0.0004 | −0.0063 | −0.0063 | 0.1262 |
| 6 | 995.9055 | 995.9060 | 995.9140 | 995.9141 | 995.7241 | −0.0004 | −0.0085 | −0.0086 | 0.1814 |
| 7 | 1302.1793 | 1302.1798 | 1302.1903 | 1302.1904 | 1301.9329 | −0.0005 | −0.0110 | −0.0111 | 0.2464 |
| 8 | 1647.3068 | 1647.3072 | 1647.3208 | 1647.3208 | 1646.9864 | −0.0004 | −0.0139 | −0.0140 | 0.3204 |
| 9 | 2030.6710 | 2030.6714 | 2030.6881 | 2030.6881 | 2030.2674 | −0.0004 | −0.0171 | −0.0171 | 0.4036 |
| 10 | 2451.5921 | 2451.5925 | 2451.6127 | 2451.6127 | 2451.0967 | −0.0004 | −0.0206 | −0.0206 | 0.4954 |
| 11 | 2909.3322 | | | 2909.3565 | 2908.7365 | | | −0.0243 | 0.5957 |
| 12 | 3403.0987 | | | 3403.1270 | 3402.3957 | | | −0.0283 | 0.7030 |
| 13 | 3932.0489 | | | 3932.0815 | 3931.2291 | | | −0.0326 | 0.8198 |
| 14 | 4495.2944 | | | 4495.3314 | | | | −0.0370 | |
| 15 | 5091.9050 | 5091.9053 | 5091.9466 | 5091.9467 | | −0.0003 | −0.0416 | −0.0417 | |
| 16 | 5720.9135 | | | 5720.9601 | | | | −0.0466 | |
| 17 | 6381.3199 | | | 6381.3715 | | | | −0.0516 | |
| 18 | 7072.0957 | | | 7072.1524 | | | | −0.0567 | |
| 19 | 7792.1880 | | | 7792.2501 | | | | −0.0621 | |
| 20 | 8540.5241 | 8540.5246 | 8540.5914 | 8540.5916 | | −0.0005 | −0.0673 | −0.0675 | |

rotational states can be described using the $J$ and $K$ rotational quantum labels as:

$$E_{JK} \sim BJ(J+1) + (C-B)K^2. \quad (1)$$

where $E_{JK}$ is the relative energy of the ro-vibrational state corresponding to its vibrational parent. Although for $H_3^+$ $J$ is always a good quantum number, due to the coupling of the rotational and the vibrational ($l$) angular momenta in this case, it has been argued [8, 105–107] that instead of using $K$, it is better to use $G = |K - l|$, which becomes a much better quantum number at low energies [8]. However, we will assign values to both.

For $l = 0$, $G = |K|$, and so the usual $(2J + 1)$-fold rotational progression arises. For $|l| > 0$, however, the$\pm l$ values double the number of the rotational excited states to $2(2J + 1)$. For $|l| > J$, there is only one rotational progression, where $G_{min} = (|l| - J) \leq G \leq G_{max} = (|l| + J)$. For $|l| \leq J$, the rotational excited states can be separated into two distinct rotational progressions [8, 107], with $0 \leq G \leq G_{max} = (J + |l|)$, and $0 \leq G' \leq G'_{max} = (J - |l|)$, and they have $(2G_{max} + 1)$ and $(2G'_{max} + 1)$ states, respectively. These two rotational progressions often have different rotational constants and a trend similar to Eq. 1

$$E_{JG} \sim BJ(J+1) + (C-B)G^2 \quad (2)$$

$$E'_{JG'} \sim B'J(J+1) + (C'-B')G'^2. \quad (3)$$

As it usually holds that $G_{max} > J$, $E_{JG}$ can become *negative*—as happens, e.g., for the $A_2''$ state, $(v_1, v_2, |l|, J, G)$=(0 2 2 1 3). This behavior is similar to the negative rotational energies observed for "quasi-structural" molecules [108] such as $H_5^+$ [109], $CH_5^+$ [110–112], $CH_4{\cdot}H_2O$ [113], $CH_4{\cdot}CH_4$, and $H_2O{\cdot}H_2O$ [114].

The presence of the two progressions requires that in addition to $G$, a new quantum number, $U$ [8, 107], has to be introduced. $U$ can take the values "u", "l", or "m" to distinguish between upper and lower energy levels with the same $(v_1, v_2, |l|, J, G)$ assignment (note, that $U$ = "l" always refers to levels within the $G'$ progression). Therefore, the rotational part of the wave function can be unambiguously described by the $(J, G, U)$ quantum labels. This, however, does not mean that we cannot assign $K$ values to each ro-vibrational state, as from the definition

of $G$, we can assign $|K| = |G - |l||$ for the unprimed progressions, and $|K| = G' + |l|$ for the primed progressions. Therefore, in the end, we characterize the rotational part using the ($J$, $G$, $U$, $K$) quantum label quartet.

For $J > 0$, $D_{3h}$ irrep labels are also linked to the quantum numbers, but it is actually $G$ which is most directly impacted (for $J = 0$, $|l| = G$). The $D_{3h}$ irrep is $A_1$ or $A_2$ if $G = 0$ (if $l = 0$, we have $A_1$ for even and $A_2$ for odd $J$ values), and for $G > 0$, similarly to $J = 0$, the degenerate pair can be labeled as $E$ unless $|l| \bmod 3 = 0$, where the $\pm\, l$ pair splits into $A_1 \oplus A_2$. For large $G$ values, especially for $G \geq 12$, the two singly degenerate levels can get closer than $10^{-5}$ cm$^{-1}$; therefore, in certain cases, $G$ values have to be taken into account when assigning $D_{3h}$ labels.

Finally, note that to further aid in the assignment of the rotational labels, the RRD overlaps of ***GENIUSH*** also provide insights into the value of $K$. This occurs through the vibrational parent being assigned (in particular, $l$) into the $G$ quantum number, as the symmetric top rigid rotor functions are labeled by $K$. This feature of the approach helped us tremendously in carrying out the task of assigning labels—so long as the RRD overlap values were significantly large.

## 3.3 Ro-vibrational energy levels

The ro-vibrational energy levels reported in this article are presented in cm$^{-1}$, relative to the zero-point vibrational energy, 4362.1726 cm$^{-1}$. The levels were obtained for each $J$, $\epsilon$, and $p$ set of values in a separate ***ScalIT*** calculation with a single PIST spectral window, usually including 70 to 120 ro-vibrational states. The number of computed levels and the highest energy level computed is summarized in Table 3 for each $J$ value. Note that these numbers include the unphysical states, and the doubly degenerate states are counted twice. In total, 105 vibrational energy levels were computed, up to 16,500 cm$^{-1}$, significantly over the isomerization barrier. For $J = 1$, the computed states (around 350 in all) covered the range up to 17,300 cm$^{-1}$. For $2 \leq J \leq 7$, around 420 to 480 levels were computed for each $J$ up to the decreasing energy limit of 15,600 to 12,600 cm$^{-1}$ with the increase of $J$. For higher $J$ values, around 300 levels were computed for each $J$. For $8 \leq J \leq 20$, the energy range increased from 10,800 cm$^{-1}$ for $J = 8$ to up to 16,700 cm$^{-1}$ for $J = 20$. All of the computed levels are included in the Supplementary Material.

In Table 2, the lowest ro-vibrational energy levels of $H_3^+$ for each $J$ up to $J = 20$ are compared with past [35, 43] calculations. The PES75K+ has been only used in our previous study [43] so far, using nuclear masses. The levels computed here are only slightly lower than those, by 3–5 × 10$^{-4}$ cm$^{-1}$ for all levels. In our previous study, we also carried out computations [43] using the GLH3P PES, just as Ref [35], as well. Those two sets of numbers are identical and slightly higher than the numbers of this work, by up to 0.07 cm$^{-1}$. Ref [35] also repeated their calculations by unequal vibrational and rotational masses, which yielded eigenvalues lower than ours, by 0.8 cm$^{-1}$ up to $J = 13$. We did not modify our masses because we prefer keeping our calculations "ab initio". In the future, we plan to do further investigations where we include non-adiabatic effects explicitly through non-adiabatic calculations with multiple PESs. [26].

TABLE 3 For each $J$ value, the total number of states computed (comp.) and labeled (lab.). Note that the former number includes the unphysical states as well, and there the doubly degenerate states are counted twice. $E_{comp}$ and $E_{lab}$ are the threshold energies for computation and labeling, respectively. As not all the states were labeled up to $E_{lab}$, a separate threshold was also included, up to which all the states are labeled ($E_{lab}' < E_{lab}$).

| $J$ | Comp | Lab | $E_{comp}$ | $E_{lab}$ | $E_{lab}'$ |
|---|---|---|---|---|---|
| 0 | 105 | 29 | 16 460.5 | 14 056.4 | 14 056.4 |
| 1 | 354 | 107 | 17 327.3 | 14 193.8 | 14 193.8 |
| 2 | 429 | 111 | 15 662.9 | 14 850.8 | 14 319.1 |
| 3 | 442 | 127 | 14 409.2 | 13 641.7 | 12 680.0 |
| 4 | 450 | 117 | 13 514.7 | 11 892.5 | 11 624.5 |
| 5 | 467 | 117 | 13 131.6 | 10 116.4 | 10 116.4 |
| 6 | 421 | 122 | 12 236.7 | 10 166.2 | 10 166.2 |
| 7 | 477 | 117 | 12 634.2 | 10 023.6 | 9019.8 |
| 8 | 302 | 113 | 10 775.2 | 10 230.3 | 9842.5 |
| 9 | 295 | 117 | 10 951.7 | 10 467.7 | 9893.7 |
| 10 | 311 | 126 | 11 398.6 | 11 077.1 | 10 187.2 |
| 11 | 293 | 135 | 11 374.0 | 11 237.6 | 10 899.2 |
| 12 | 300 | 98 | 11 840.5 | 10 713.4 | 10 673.5 |
| 13 | 298 | 102 | 12 289.8 | 11 132.4 | 11 132.4 |
| 14 | 301 | 102 | 12 845.1 | 12 035.7 | 11 789.9 |
| 15 | 295 | 108 | 13 373.0 | 12 990.1 | 12 168.4 |
| 16 | 300 | 66 | 14 013.6 | 12 695.7 | 11 445.3 |
| 17 | 311 | 70 | 14 759.9 | 13 694.8 | 12 067.3 |
| 18 | 300 | 70 | 15 268.0 | 14 720.9 | 12 845.8 |
| 19 | 303 | 61 | 15 959.9 | 14 263.7 | 13 409.8 |
| 20 | 310 | 58 | 16 736.1 | 14 997.5 | 14 213.4 |

The main focus of this work is, however, to provide vibrational and rotational quantum labels for as many states as possible. In our previous study [43], although $D_{3h}$ irrep labels were provided for selected $J$ values ($J = 10, 20, 30, 40, 46$) up to $J = 46$, we only provided a limited number of vibrational and rotational quantum label assignments. Only low $J$ values $0 \leq J \leq 5$ and $J = 10$ were considered, and even those were mostly restricted to up to 8,000–9,000 cm$^{-1}$, so overall, below the isomerization limit. Only for $J = 0$ and 1 did we go above 10,000 cm$^{-1}$. Here, we pushed our efforts further with the help of wave function overlaps and provided assignments for almost all states below 10,000 cm$^{-1}$. In Table 3, we summarize the number of states labeled in this work for each $J$ value separately as well as include the labeling threshold, $E_{lab}$. As for most $J$ values, not all of the levels were assigned up to the given threshold energy, we separately include the energy value up to which all states are labeled, $E_{lab}'$.

TABLE 4 Suggested vibrational ($v_1$, $v_2$, $|l|$) and rotational ($J$, $G$, $U$, $K$) reassignments of $H_3^+$ MARVEL energy levels.

| MARVEL | | | | | | | | | *ScalIT* | | | | | | | |
|---|---|---|---|---|---|---|---|---|---|---|---|---|---|---|---|---|
| **Level** | **Sym** | $v_1$ | $v_2$ | $l_2$ | $J$ | $G$ | $U$ | $K$ | **Level** | $\delta E$ | $v_1$ | $v_2$ | $l_2$ | $G$ | $U$ | $K$ |
| 7008.75 | $E'$ | 0 | 1 | 1 | 11 | 7 | u | 6 | 7009.14 | 0.40 | 0 | 1 | 1 | 5 | l | 6 |
| 7676.65 | $E''$ | 1 | 1 | 1 | 9 | 8 | u | 7 | 7677.00 | 0.34 | 1 | 1 | 1 | 8 | l | 9 |
| 8135.75 | $E''$ | 0 | 2 | 2 | 9 | 5 | l | 7 | 8136.23 | 0.49 | 0 | 2 | 0 | 1 | m | 1 |
| 8176.10 | $E''$ | 0 | 2 | 0 | 9 | 1 | m | 1 | 8176.60 | 0.49 | 0 | 2 | 2 | 5 | l | 7 |
| 8532.45 | $E'$ | 1 | 2 | 2 | 4 | 2 | l | 4 | 8533.20 | 0.75 | 1 | 2 | 0 | 2 | m | 2 |
| 8872.11 | $E''$ | 0 | 2 | 2 | 9 | 1 | u | 1 | 8872.72 | 0.61 | 1 | 1 | 1 | 2 | l | 3 |
| 8924.60 | $E''$ | 1 | 1 | 1 | 9 | 2 | l | 3 | 8925.22 | 0.62 | 0 | 2 | 2 | 1 | u | 1 |
| 9158.44 | $E'$ | 0 | 3 | 1 | 7 | 1 | l | 2 | 9159.14 | 0.70 | 0 | 3 | 3 | 7 | m | 4 |
| 9251.70 | $E''$ | 0 | 2 | 2 | 11 | 7 | u | 5 | 9252.28 | 0.58 | 0 | 2 | 2 | 7 | l | 9 |
| 9313.04 | $E'$ | 1 | 2 | 2 | 6 | 4 | u | 2 | 9313.88 | 0.84 | 2 | 1 | 1 | 7 | m | 6 |
| 9409.49 | $A_2''$ | 0 | 3 | 3 | 6 | 0 | m | 3 | 9410.28 | 0.79 | 1 | 2 | 0 | 3 | m | 3 |
| 9428.61 | $E'$ | 0 | 3 | 3 | 6 | 1 | u | 2 | 9429.39 | 0.78 | 1 | 2 | 0 | 2 | m | 2 |
| 9497.27 | $A_2''$ | 0 | 2 | 2 | 12 | 9 | u | 7 | 9497.85 | 0.58 | 0 | 2 | 2 | 9 | l | 11 |
| 9643.34 | $E''$ | 0 | 2 | 2 | 12 | 7 | l | 9 | 9643.78 | 0.44 | 0 | 2 | 0 | 7 | m | 7 |
| 9661.29 | $A_2'$ | 1 | 2 | 0 | 7 | 6 | m | 6 | 9661.61 | 0.32 | 1 | 2 | 2 | 6 | m | 4 |
| 11 027.20 | $E'$ | 0 | 5 | 3 | 2 | 5 | m | 2 | 11 028.01 | 0.82 | 0 | 5 | 1 | 1 | l | 2 |
| 11 108.27 | $E'$ | 0 | 5 | 1 | 2 | 1 | l | 2 | 11 109.10 | 0.83 | 0 | 5 | 3 | 5 | m | 2 |
| 11 188.65 | $E''$ | 2 | 2 | 2 | 3 | 1 | u | 1 | 11 189.51 | 0.87 | 0 | 5 | 1 | 2 | l | 3 |
| 11 207.16 | $E''$ | 0 | 5 | 1 | 3 | 2 | l | 3 | 11 208.19 | 1.03 | 2 | 2 | 2 | 1 | u | 1 |
| 11 298.59 | $E'$ | 0 | 5 | 3 | 3 | 5 | m | 2 | 11 299.41 | 0.82 | 0 | 5 | 1 | 1 | l | 2 |
| 11 369.04 | $A_2'$ | 0 | 5 | 1 | 4 | 3 | u | 2 | 11 369.88 | 0.84 | 0 | 5 | 1 | 3 | l | 4 |
| 11 484.07 | $E'$ | 0 | 5 | 1 | 3 | 1 | l | 2 | 11 484.92 | 0.86 | 0 | 5 | 3 | 5 | m | 2 |
| 11 771.38 | $E'$ | 0 | 5 | 5 | 2 | 5 | m | 0 | 11 772.46 | 1.08 | 0 | 5 | 5 | 7 | m | 2 |
| 11 946.50 | $E'$ | 1 | 4 | 0 | 2 | 2 | m | 2 | 11 947.55 | 1.05 | 0 | 5 | 5 | 5 | m | 0 |
| 11 984.97 | $E''$ | 0 | 5 | 3 | 3 | 2 | m | 1 | 11 985.99 | 1.02 | 0 | 5 | 5 | 2 | m | 3 |
| 11 957.57 | $E''$ | 0 | 5 | 3 | 2 | 2 | m | 1 | 11 958.60 | 1.03 | 0 | 5 | 5 | 4 | m | 1 |
| 12 058.87 | $E'$ | 0 | 5 | 5 | 3 | 5 | m | 0 | 12 059.94 | 1.07 | 0 | 5 | 5 | 7 | m | 2 |
| 12 208.46 | $A_2''$ | 0 | 5 | 3 | 3 | 0 | m | 3 | 12 209.51 | 1.05 | 0 | 5 | 5 | 6 | m | 1 |
| 12 267.00 | $E''$ | 1 | 4 | 0 | 3 | 1 | m | 1 | 12 268.10 | 1.10 | 0 | 5 | 5 | 4 | m | 1 |
| 12 506.09 | $E''$ | 1 | 4 | 4 | 1 | 5 | m | 1 | 12 507.17 | 1.08 | 0 | 6 | 0 | 1 | m | 1 |
| 12 687.29 | $E'$ | 1 | 4 | 4 | 1 | 4 | m | 0 | 12 688.34 | 1.05 | 0 | 6 | 2 | 2 | m | 0 |
| 12 840.66 | $A_2'$ | 1 | 4 | 4 | 3 | 6 | m | 2 | 12 841.77 | 1.11 | 2 | 3 | 1 | 2 | m | 2 |
| 13 135.71 | $E'$ | 2 | 3 | 3 | 2 | 1 | m | 2 | 13 136.77 | 1.06 | 0 | 6 | 2 | 2 | m | 0 |

During this work, 2,210 ro-vibrational levels of $H_3^+$ have been assigned ($v_1$, $v_2$, $|l|$) vibrational and ($J$, $G$, $U$, $K$) rotational quantum labels. All of the labeled energy levels and their assignments are included in the Supplementary Material. For 1,571 of these levels, quantum labels have not been assigned before, while the remaining 639 levels are part of the 652 experimental ro-vibrational levels currently included in MARVEL. For 33 of these MARVEL levels, new vibrational ($v_1$, $v_2$, $|l|$) and/or rotational ($J$, $G$, $U$, $K$) assignments have been proposed (see Table 4).

In order to obtain all the quantum labels presented here, our approach has been adapted keeping in mind the difficulties we faced in Ref. [43]. Based on the energy formula of Eqs 2, 3, one would expect a somewhat regular behavior in the shifting of the rotationally excited energy levels belonging to the same vibrational parent. However, this seems to hold only for the $l = 0$ cases. In Figure 1, the change of $B$ rotational constant is illustrated as $J$ is increased. Each rotational progression belonging to a vibrational state can be characterized by a slightly different $B$ rotational constant, which also shifts slightly by the increase of $J$. As the vibrational excitation increases, this shift becomes more significant (e.g. in case of 0, 2, 0 and 0, 4, 0). However, for the $l >$ 0 vibrational parents, this shift can be more chaotic (see Figure 2)

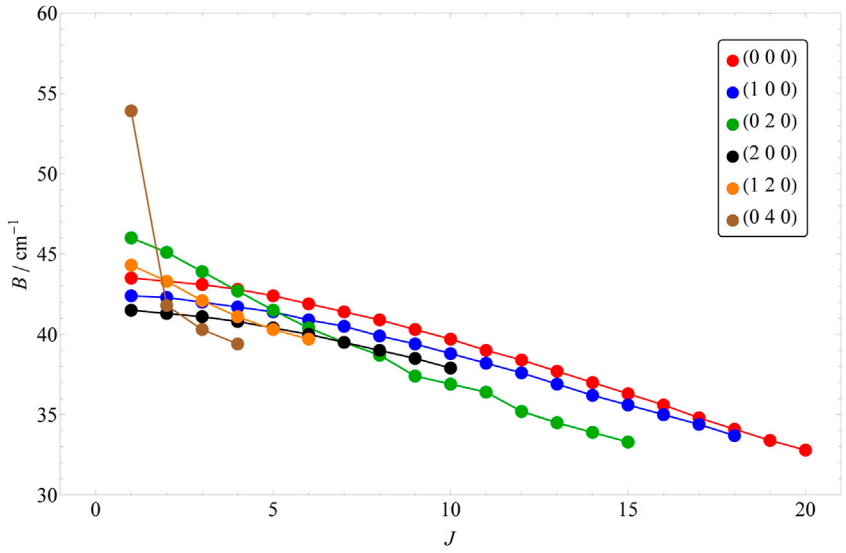


FIGURE 1
The shift of the $B$ rotational constants with the increase of the $J$ value for the first 6 $l$ = 0 vibrational parents.

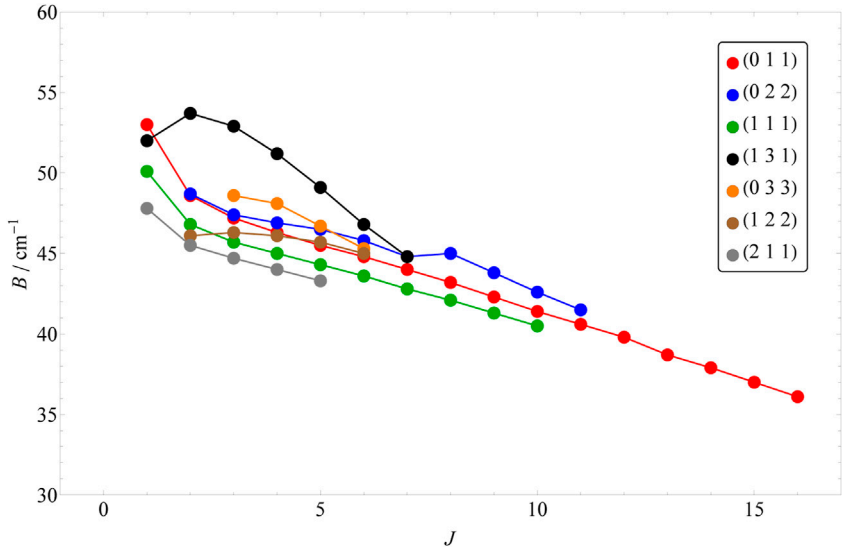


FIGURE 2
The shift of the $B$ rotational constants with the increase of the $J$ value for the first 7 $l$ > 0 vibrational parents. The numbers included here correspond to the $G$ progression.

and it is different for the two distinct rotational progressions, assigned to $G$ and $G'$ (see Figures 2, 3). For the (1, 3, 1) vibrational parent, e.g., the shift seems to first be positive and then it turns negative as it is in all other cases for both progressions. The $G$ = 0 energy levels of the first 13 vibrational states up to $J$ = 20 are listed in Table 5, while $G'$ = 0 energy levels of the first 7 $l$ > 0 vibrational states up to $J$ = 16 are included in Table 6.

Using the RRD method [57] of ***GENIUSH*** to compute wave function overlaps and assign vibrational parents we can push the labeling a lot further than simply relying on the

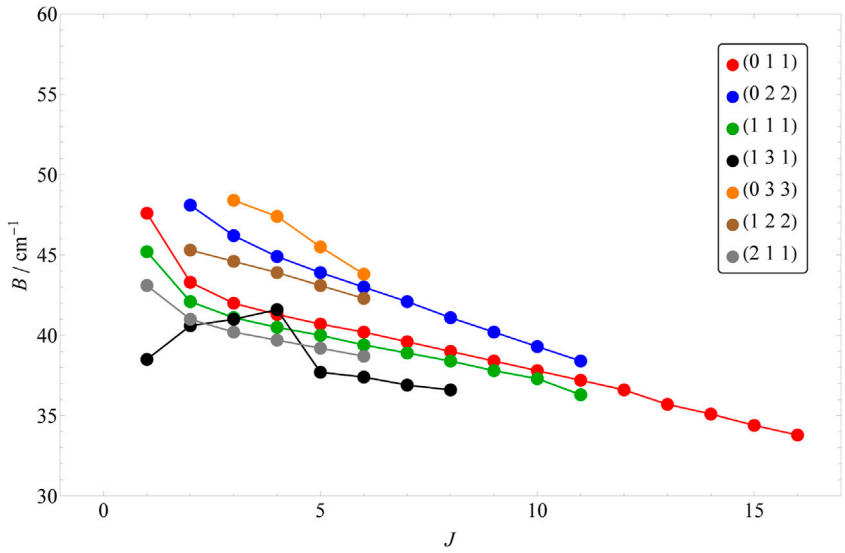


FIGURE 3
The shift of the $B$ rotational constants with the increase of the $J$ value for the first 7 $l > 0$ vibrational parents. The numbers included here correspond to the $G'$ progression.

TABLE 5 The $G = 0$ energy levels of the first 13 vibrational states ($v_1$, $v_2$, $|l|$) of $H_3^+$ up to $J = 20$.

| $J$ | 0,0,0 | 0,1,1 | 1,0,0 | 0,2,0 | 0,2,2 | 1,1,1 | 2,0,0 | 0,3,1 | 0,3,3 | 1,2,0 | 1,2,2 | 2,1,1 | 0,4,0 |
|---|---|---|---|---|---|---|---|---|---|---|---|---|---|
| 0 | 0.0 | | 3178.7 | 4778.7 | | | 6262.8 | | | 7770.1 | | | 9002.4 |
| 1 | 87.0 | 2627.5 | 3263.5 | 4870.6 | | 5655.0 | 6345.8 | 7110.7 | | 7858.7 | | 8584.5 | 9110.3 |
| 2 | 259.9 | 2813.0 | 3432.3 | 5049.3 | 5290.7 | 5835.9 | 6510.7 | 7328.7 | | 8029.8 | 8147.6 | 8762.2 | 9253.3 |
| 3 | 516.9 | 3087.6 | 3683.2 | 5305.9 | 5567.8 | 6103.7 | 6755.8 | 7641.7 | 7869.3 | 8275.5 | 8426.2 | 9024.8 | 9486.6 |
| 4 | 855.2 | 3447.3 | 4013.4 | 5632.3 | 5937.1 | 6454.3 | 7078.3 | 8031.5 | 8248.4 | 8592.0 | 8793.6 | 9368.4 | 9790.8 |
| 5 | 1271.3 | 3887.0 | 4419.6 | 6023.5 | 6392.3 | 6883.0 | 7475.2 | 8478.8 | 8686.6 | 8978.6 | 9241.9 | 9788.4 | |
| 6 | 1761.2 | 4401.3 | 4898.0 | 6476.7 | 6922.0 | 7384.5 | 7942.6 | 8972.9 | 9189.5 | 9437.8 | 9761.4 | | |
| 7 | 2320.5 | 4984.2 | 5444.4 | 6990.2 | 7505.5 | 7953.2 | 8476.4 | 9513.2 | | | | | |
| 8 | 2944.3 | 5629.4 | 6054.2 | 7566.0 | 8235.5 | 8583.5 | 9072.4 | | | | | | |
| 9 | 3627.7 | 6330.4 | 6722.9 | 8146.3 | 8940.7 | 9269.7 | 9726.1 | | | | | | |
| 10 | 4365.7 | 7080.8 | 7445.8 | 8836.7 | 9689.7 | 10 006.5 | 10 433.1 | | | | | | |
| 11 | 5153.4 | 7883.3 | 8218.5 | 9586.4 | | | | | | | | | |
| 12 | 5985.6 | 8735.0 | 9036.9 | | | | | | | | | | |
| 13 | 6857.9 | 9574.1 | 9897.1 | | | | | | | | | | |
| 14 | 7765.7 | 10 471.3 | | | | | | | | | | | |
| 15 | 8704.9 | | | | | | | | | | | | |
| 16 | 9671.9 | | | | | | | | | | | | |
| 17 | 10 663.6 | | | | | | | | | | | | |
| 18 | 11 677.3 | | | | | | | | | | | | |
| 19 | 12 710.4 | | | | | | | | | | | | |
| 20 | 13 760.6 | | | | | | | | | | | | |

TABLE 6 The $G' = 0$ energy levels of the first 7 $l > 0$ vibrational states ($v_1$, $v_2$, $|l|$) of $H_3^+$ up to $J = 16$.

| $J$ | 0,1,1 | 0,2,2 | 1,1,1 | 0,3,1 | 0,3,3 | 1,2,2 | 2,1,1 |
|---|---|---|---|---|---|---|---|
| 1 | 2616.9 | | 5645.3 | 7083.6 | | | 8575.2 |
| 2 | 2781.5 | 5287.3 | 5807.4 | 7250.0 | | 8142.8 | 8734.8 |
| 3 | 3026.1 | 5552.3 | 6048.1 | 7498.6 | 7867.0 | 8406.6 | 8971.5 |
| 4 | 3347.9 | 5897.3 | 6364.6 | 7839.5 | 8235.1 | 8748.9 | 9282.6 |
| 5 | 3743.4 | 6316.6 | 6753.7 | 8138.1 | 8651.9 | 9164.2 | 9664.7 |
| 6 | 4208.7 | 6804.2 | 7211.5 | 8577.3 | 9125.6 | 9647.0 | 10 114.1 |
| 7 | 4739.5 | 7354.0 | 7734.2 | 9075.2 | | | |
| 8 | 5331.3 | 7960.0 | 8317.8 | 9639.2 | | | |
| 9 | 5979.5 | 8616.7 | 8959.3 | | | | |
| 10 | 6679.6 | 9318.7 | 9660.7 | | | | |
| 11 | 7427.8 | 10 063.2 | 10 351.3 | | | | |
| 12 | 8224.1 | | | | | | |
| 13 | 9020.0 | | | | | | |
| 14 | 9891.7 | | | | | | |
| 15 | 10 788.5 | | | | | | |
| 16 | 11 714.8 | | | | | | |

energy progressions. However, after a certain point in the vibrational and/or the rotational energy excitation, the mixing of the wave functions becomes simply too much for the vibrational parents to be unambiguously identified. For low $J$ values, up to $J = 6$, we were able to get past the isomerization barrier, and in most cases, we could continue on even further. As the rotational excitation increases, the highest vibrational parent we can possibly assign is also decreasing. From $J = 7$ to 10, we are barely reaching the barrier to linearity, while as $J$ increases further, the rotational energy contribution is also getting bigger, therefore we are again getting past the isomerization barrier (see Table 3). Different vibrational parents also behave differently, e.g. the overlaps of the (1,2,0) state breaks down a lot sooner than those of the next few higher-lying vibrational states. The more spread out progressions are also more difficult to assign fully including all the states within the progression. Although the progression belonging to (1,0,0) can be fully identified up to $J = 18$, in the progression of (0,1,1) we already start missing levels at $J = 16$. The ground vibrational state is the only vibrational parent for which all the states were found within the progressions for each $J$ up to $J = 20$. This, however, might not be possible for $J > 20$ values.

In certain cases, it can be observed that the $G = 0$ (or $G' = 0$) level is not the lowest level of the progression, which seemingly results in negative rotational excitations [108]. This happens for both higher vibrational excitations [e.g., for (0,5,1) at $J = 1$], higher rotational excitation (e.g., for (0,1,1) at $J = 11$), or for both [e.g., for (0,3,3) at $J = 3$ and for (0,3,1) at $J = 6$]. In certain cases, this reversing of the energy levels occurs sooner for the $G'$ progression [e.g., for (0,3,1) at $J = 5$].

# 4 Discussion

In this article, we computed ro-vibrational energy levels and wave functions for the $H_3^+$ molecular ion using a recently developed PES [25] and the ***ScalIT*** suite of parallel codes. The calculations included every single $J$ value up to $J = 20$, and for each $J$, all of the levels were computed up to the barrier of linearity or higher. The convergence accuracy of our calculations is further improved, now reaching up to a few $10^{-5}$ cm$^{-1}$ (or better). Our work has also been compared to previous works using different potential energy surfaces and different masses. Among the nuclear mass computations, the numbers of the present work were the lowest, signaling that we are still operating in the "basis set truncation error-dominated regime" where the numerical convergence is variational from above.

In addition, we carried out vibrational ($v_1$, $v_2$, $|l|$) and rotational ($J$, $G$, $U$, $K$) quantum label assignments of ro-vibrational energy levels for more than 2,200 states. To enable this, ***GENIUSH*** calculations were also carried out with lower accuracy to obtain ro-vibrational wave functions, which were then used to compute wave function overlaps within the framework of the rigid rotor decomposition method. These RRD overlaps helped greatly to identify the vibrational parents. As part of our efforts, we suggested new vibrational ($v_1$, $v_2$, $|l|$) and rotational ($J$, $G$, $U$, $K$) reassignments for certain energy levels within the MARVEL database. We are hoping that the results of this work can be used to further improve previous efforts toward creating spectroscopic line lists (based on both theoretical and experimental data), through the list of all labeled energy levels as provided in the Supplementary Material of this article.

# Data availability statement

The original contributions presented in the study are included in the article/Supplementary Material; further inquiries can be directed to the corresponding author.

# Author contributions

JS and BP designed the research, JS carried out the calculations and analyzed the data, JS and BP discussed the results, JS and BP wrote the manuscript, and BP provided funding.

# Funding

This work was supported by the National Science Foundation (CHE-1665370), and the Robert A. Welch Foundation (D-1523).

## Acknowledgments

The authors also gratefully acknowledge the Texas Tech University High Performance Computing Center for the use of the Quanah cluster and the Texas Advanced Computing Center for the use of the Lonestar5 and Frontera clusters.

## Conflict of interest

The authors declare that the research was conducted in the absence of any commercial or financial relationships that could be construed as a potential conflict of interest.

## Publisher's note

All claims expressed in this article are solely those of the authors and do not necessarily represent those of their affiliated organizations, or those of the publisher, the editors, and the reviewers. Any product that may be evaluated in this article, or claim that may be made by its manufacturer, is not guaranteed or endorsed by the publisher.

## Supplementary material

The Supplementary Material for this article can be found online at: https://www.frontiersin.org/articles/10.3389/fphy.2022.996001/full#supplementary-material

## References

1. Miller S, Tennyson J, Geballe TR, Stallard T. Thirty years of $H_3^+$ astronomy. *Rev Mod Phys* (2020) 92:035003. doi:10.1103/revmodphys.92.035003

2. Snow TP, McCall BJ. Diffuse atomic and molecular clouds. *Annu Rev Astron Astrophys* (2006) 44:367–414. doi:10.1146/annurev.astro.43.072103.150624

3. Miller S, Tennyson J, Lepp S, Dalgarno A. Identification of features due to $H_3^+$ in the infrared spectrum of supernova 1987A. *Nature* (1992) 355:420–2. doi:10.1038/355420a0

4. Miller S, Achilleos N, Ballester GE, Geballe TR, Joseph RD, Prange R, et al. The role of $H_3^+$ in planetary atmospheres. *Philosophical Trans R Soc Lond Ser A: Math Phys Eng Sci* (2000) 358:2485–502. doi:10.1098/rsta.2000.0662

5. Koskinen TT, Aylward AD, Miller S. A stability limit for the atmospheres of giant extrasolar planets. *Nature* (2007) 450:845–8. doi:10.1038/nature06378

6. Carrington A, Buttenshaw J, Kennedy R. Observation of the infrared spectrum of $H_3^+$ at its dissociation limit. *Mol Phys* (1982) 45:753–8. doi:10.1080/00268978200100591

7. Carrington A, McNab IR, West YD. Infrared predissociation spectrum of the $H_3^+$ ion. II. *J Chem Phys* (1993) 98:1073–92. doi:10.1063/1.464331

8. Lindsay C, McCall BJ. Comprehensive evaluation and compilation of $H_3^+$ spectroscopy. *J Mol Spectrosc* (2001) 210:60–83. doi:10.1006/jmsp.2001.8444

9. Schiffels P, Alijah A, Hinze J. Rovibrational states of $H_3^+$. Part 1: The energy region below 9,000 $cm^{-1}$ and modelling of the non-adiabatic effects. *Mol Phys* (2001) 101:175. doi:10.1080/00268970210158687

10. Schiffels P, Alijah A, Hinze J. Rovibrational states of $H_3^+$. Part 2: The energy region between 9,000 $cm^{-1}$ and 13,000 $cm^{-1}$ including empirical corrections for the non-adiabatic effects. *Mol Phys* (2001) 101:189. doi:10.1080/00268970210158713

11. Asvany O, Hugo E, Schlemmer S, Muller F, Kuhnemann F, Schiller S, et al. Overtone spectroscopy of $H_2D^+$ and $D_2H^+$ using laser induced reactions. *J Chem Phys* (2007) 127:154317. doi:10.1063/1.2794331

12. Pavanello M, Adamowicz L, Alijah A, Zobov NF, Mizus II, Polyansky OL, et al. Precision measurements and computations of transition energies in rotationally cold triatomic hydrogen ions up to the midvisible spectral range. *Phys Rev Lett* (2012) 108:023002. doi:10.1103/physrevlett.108.023002

13. Furtenbacher T, Szidarovszky T, Mátyus E, Fábri C, Csaszár AG. Analysis of the rotational–vibrational states of the molecular ion $H_3^+$. *J Chem Theor Comput* (2013) 9:5471–8. doi:10.1021/ct4004355

14. Furtenbacher T, Szidarovszky T, Fábri C, Császár AG. MARVEL analysis of the rotational–vibrational states of the molecular ions $H_2D^+$ and $D_2H^+$. *Phys Chem Chem Phys* (2013) 15:10181. doi:10.1039/c3cp44610g

15. Császár AG, Furtenbacher T. Spectroscopic networks. *J Mol Spectrosc* (2011) 266:99–103. doi:10.1016/j.jms.2011.03.031

16. Császár AG, Furtenbacher T, Árendás P. Small molecules—big Data. *J Phys Chem A* (2016) 120:8949–69. doi:10.1021/acs.jpca.6b02293

17. Furtenbacher T, Császár AG, Tennyson J. Marvel: Measured active rotational–vibrational energy levels. *J Mol Spectrosc* (2007) 245:115–25. doi:10.1016/j.jms.2007.07.005

18. Furtenbacher T, Császár AG. Marvel: Measured active rotational–vibrational energy levels. II. Algorithmic improvements. *J Quant Spectrosc Radiat Transf* (2012) 113:929–35. doi:10.1016/j.jqsrt.2012.01.005

19. Marvel online (2022). Available from: https://kkrk.chem.elte.hu/marvelonline/index.php (accessed 07 11, 2022).

20. Cencek W, Rychlewski J, Jaquet R, Kutzelnigg W. Sub-microhartree accuracy potential energy surface for $H_3^+$ including adiabatic and relativistic effects. I. Calculation of the potential points. *J Chem Phys* (1998) 108:2831–6. doi:10.1063/1.475702

21. Jaquet R, Cencek W, Kutzelnigg W, Rychlewski J. Sub-microhartree accuracy potential energy surface for $H_3^+$ including adiabatic and relativistic effects. II. Rovibrational analysis for $H_3^+$ and $D_3^+$. *J Chem Phys* (1998) 108:2837–46. doi:10.1063/1.475703

22. Polyansky O, Prosmiti R, Klopper W, Tennyson J. An accurate, global, *ab initio* potential energy surface for the $H_3^+$ molecule. *Mol Phys* (2000) 98:261–73. doi:10.1080/00268970009483290

23. Velilla L, Lepetit B, Aguado A, Beswick J, Paniagua M. The $H_3^+$ rovibrational spectrum revisited with a global electronic potential energy surface. *J Chem Phys* (2008) 129:084307. doi:10.1063/1.2973629

24. Pavanello M, Adamowicz L, Alijah A, Zobov NF, Mizus II, Polyansky OL, et al. Calibration-quality adiabatic potential energy surfaces for $H_3^+$ and its isotopologues. *J Chem Phys* (2012) 136:184303. doi:10.1063/1.4711756

25. Mizus II, Polyansky OL, McKemmish LK, Tennyson J, Alijah A, Zobov NF. A global potential energy surface for $H_3^+$. *Mol Phys* (2019) 117:1663–72. doi:10.1080/00268976.2018.1554195

26. Aguado A, Roncero O, Sanz-Sanz C. Three states global fittings with improved long range: Singlet and triplet states of $H_3^+$. *Phys Chem Chem Phys* (2021) 113. doi:10.1039/D0CP04100A

27. Miller S, Tennyson J. Calculation of the high angular momentum dissociation limit for $H_3^+$ and $H_2D^+$. *Chem Phys Lett* (1988) 145:117–20. doi:10.1016/0009-2614(88)80161-1

28. Kozin IN, Roberts RM, Tennyson J. Symmetry and structure of rotating $H_3^+$. *J Chem Phys* (1999) 111:140–50. doi:10.1063/1.479260

29. Kostin MA, Polyansky OL, Tennyson J, Mussa HY. Rotation-vibration states of $H_3^+$ at dissociation. *J Chem Phys* (2003) 118:3538–42. doi:10.1063/1.1539034

30. Munro JJ, Ramanlal J, Tennyson J, Mussa HY. Properties of high-lying vibrational states of the molecular ion. *Mol Phys* (2006) 104:115–25. doi:10.1080/00268970500399648

31. Bachorz RA, Cencek W, Jaquet R, Komasa J. Rovibrational energy levels of $H_3^+$ with energies above the barrier to linearity. *J Chem Phys* (2009) 131:024105. doi:10.1063/1.3167795

32. Alijah A. Accurate calculations and assignments of above-barrier states of up to. *J Mol Spectrosc* (2010) 264:111–9. doi:10.1016/j.jms.2010.09.009

33. Szidarovszky T, Császár AG, Czakó G. On the efficiency of treating singularities in triatomic variational vibrational computations. The vibrational states of $H_3^+$ up to dissociation. *Phys Chem Chem Phys* (2010) 12:8373. doi:10.1039/c001124j

34. Diniz LG, Alijah JRMA, Pavanello M, Adamowicz L, Polyansky OL, Tennyson J, et al. Vibrationally and rotationally nonadiabatic calculations on $H_3^+$ using coordinate-dependent vibrational and rotational masses. *Phys Rev A (Coll Park)* (2013) 88:032506. doi:10.1103/physreva.88.032506

35. Jaquet R, Carrington T, Jr. Using a nondirect product basis to compute $J > 0$ rovibrational states of $H_3^+$. *J Phys Chem A* (2013) 117:9493–500. doi:10.1021/jp312027s

36. Jaquet R. Investigation of the highest bound ro-vibrational states of $H_3^+$, $DH_2^+$, $HD_2^+$, $D_3^+$, and $T_3^+$: Use of a non-direct product basis to compute the highest allowed $J > 0$ states. *Mol Phys* (2013) 111:2606–16. doi:10.1080/00268976.2013.818727

37. Mátyus E, Szidarovszky T, Császár AG. Modelling non-adiabatic effects in $H_3^+$: Solution of the rovibrational Schrödinger equation with motion-dependent masses and mass surfaces. *J Chem Phys* (2014) 141:154111. doi:10.1063/1.4897566

38. Jaquet R, Khoma MV. Investigation of nonadiabatic effects for the vibrational spectrum of a triatomic molecule: The use of a single potential energy surface with distance-Dependent masses for $H_3^+$. *J Phys Chem A* (2017) 121:7016–30. doi:10.1021/acs.jpca.7b04703

39. Jaquet R, Khoma MV. Investigation of non-adiabatic effects for the ro-vibrational spectrum of $H_3^+$: The use of a single potential energy surface with geometry-dependent nuclear masses. *Mol Phys* (2018) 116:3507–18. doi:10.1080/00268976.2018.1464225

40. Tennyson J, Polyansky OL, Zobov NF, Alijah A, Császár AG. High-accuracy calculations of the rotation-vibration spectrum of $H_3^+$. *J Phys B: Mol Opt Phys* (2017) 50:232001. doi:10.1088/1361-6455/aa8ca6

41. Jaquet R, Lesiuk M. Analysis of QED and non-adiabaticity effects on the rovibrational spectrum of $H_3^+$ using geometry-dependent effective nuclear masses. *J Chem Phys* (2020) 152:104109. doi:10.1063/1.5144293

42. Sarka J, Poirier B, Szalay V, Császár AG. On neglecting Coriolis and related couplings in first-principles rovibrational spectroscopy: Considerations of symmetry, accuracy, and simplicity. II. Case studies for $H_2O$ isotopologues, $H_3^+$, $O_3$, and $NH_3$. *Spectrochim Acta A Mol Biomol Spectrosc* (2021) 250:119164. doi:10.1016/j.saa.2020.119164

43. Sarka J, Das D, Poirier B. Calculation of rovibrational eigenstates of $H_3^+$ using *ScalIT*. *AIP Adv* (2021) 11:045033. doi:10.1063/5.0047823

44. Moss RE. On the adiabatic and non-adiabatic corrections in the ground electronic state of the hydrogen molecular cation. *Mol Phys* (1996) 89:195–210. doi:10.1080/002689796174083

45. Diniz LG, Alijah A, Mohallem JR. Core-mass nonadiabatic corrections to molecules: $H_2$, $H_2^+$, and isotopologues. *J Chem Phys* (2012) 137:164316. doi:10.1063/1.4762442

46. Huestic DL. Hydrogen collisions in planetary atmospheres, ionospheres, and magnetospheres. *Planet Space Sci* (2008) 56:1733. doi:10.1016/j.pss.2008.07.012

47. McKemmish LK, Tennyson J. General mathematical formulation of scattering processes in atom–diatomic collisions in the RmatReact methodology. *Phil Trans R Soc A* (2019) 377:20180409. doi:10.1098/rsta.2018.0409

48. Höveler K, Deiglmayr J, Agner JA, Schmutz H, Merkt F. The $H_2^+$ + HD reaction at low collision energies: $H_3^+/H_2D^+$ branching ratio and product-kinetic-energy distributions. *Phys Chem Chem Phys* (2021) 23:2676–85. doi:10.1039/d0cp06107g

49. Huang X, Schwenke DW, Lee TJ. Highly accurate potential energy surface, dipole moment surface, rovibrational energy levels, and infrared line list for $^{32}S^{16}O_2$ up to 8,000 $cm^{-1}$. *J Chem Phys* (2014) 140:114311. doi:10.1063/1.4868327

50. Kumar P, Jiang B, Guo H, Klos J, Alexander MH, Poirier B. Photoabsorption assignments for the $C^1B_2 \leftarrow X^1A_1$ vibronic transitions of $SO_2$, using new ab initio potential energy and transition Dipole surfaces. *J Phys Chem A* (2017) 121:1012–21. doi:10.1021/acs.jpca.6b12958

51. Kao L, Oka T, Miller S, Tennyson J. A table of astronomically important ro-vibrational transitions for the $H_3^+$ molecular ion. *Astrophys J Suppl Ser* (1991) 77:317. doi:10.1086/191606

52. Neale L, Miller S, Tennyson J. Spectroscopic properties of the $H_3^+$ molecule: A new calculated line list. *Astrophys J* (1996) 464:516. doi:10.1086/177341

53. Mizus II, Alijah A, Zobov NF, Lodi L, Kyuberis AA, Yurchenko SN, et al. ExoMol molecular line lists – XX. A comprehensive line list for H3+. *Mon Not R Astron Soc* (2017) 468:1717–25. doi:10.1093/mnras/stx502

54. Tennyson J, Kostin MA, Barletta P, Harris GJ, Polyansky OL, Ramanlal J, et al. DVR3D: A program suite for the calculation of rotation–vibration spectra of triatomic molecules. *Computer Phys Commun* (2004) 163:85–116. doi:10.1016/j.cpc.2003.10.003

55. Tennyson J. Perspective: Accurate ro-vibrational calculations on small molecules. *J Chem Phys* (2016) 145:120901. doi:10.1063/1.4962907

56. Tennyson J, Yurchenko SN. The ExoMol project: Software for computing large molecular line lists. *Int J Quan Chem* (2017) 117:92–103. doi:10.1002/qua.25190

57. Mátyus E, Fábri C, Szidarovszky T, Czakó G, Allen WD, Császár AG. Assigning quantum labels to variationally computed rotational-vibrational eigenstates of polyatomic molecules. *J Chem Phys* (2010) 133:034113. doi:10.1063/1.3451075

58. Chen W, Poirier B. Parallel implementation of efficient preconditioned linear solver for grid-based applications in chemical physics. I: Block Jacobi diagonalization. *J Comput Phys* (2006) 219:185–97. doi:10.1016/j.jcp.2006.04.012

59. Chen W, Poirier B. Parallel implementation of efficient preconditioned linear solver for grid-based applications in chemical physics. II: QMR linear solver. *J Comput Phys* (2006) 219:198–209. doi:10.1016/j.jcp.2006.03.031

60. Chen W, Poirier B. Parallel implementation of an efficient preconditioned linear solver for grid-based applications in chemical physics. III: Improved parallel scalability for sparse matrix–vector products. *J Parallel Distrib Comput* (2010) 70:779–82. doi:10.1016/j.jpdc.2010.03.008

61. Chen W, Poirier B. Quantum dynamics on massively parallel computers: efficient numerical implementation for preconditioned linear solvers and eigensolvers. *J Theor Comput Chem* (2010) 9:825–46. doi:10.1142/s021963361000602x

62. Petty C, Poirier B. Using ScalIT for performing accurate rovibrational spectroscopy calculations for triatomic molecules: A practical guide. *Appl Math (Irvine)* (2014) 5:2756–63. doi:10.4236/am.2014.517263

63. Poirier B, Light JC. Phase space optimization of quantum representations: Direct-product basis sets. *J Chem Phys* (1999) 111:4869–85. doi:10.1063/1.479747

64. Poirier B, Light JC. Phase space optimization of quantum representations: Three-body systems and the bound states of HCO. *J Chem Phys* (2001) 114:6562–71. doi:10.1063/1.1354181

65. Poirier B. Research topic "proton transfer processes in biological reactions: a computational approach" frontiers in chemistry journal. *Found Phys* (2001) 31:1581–610. doi:10.1023/a:1012642832253

66. Bian W, Poirier B. Accurate and highly efficient calculation of the $O(^1D)HCl$ vibrational bound states, using A combination of methods. *J Theor Comput Chem* (2003) 2:583–97. doi:10.1142/s0219633603000768

67. Light J, Carrington T, Jr.. Discrete-variable representations and their utilization *Adv Chem Phys* (2000) 114:263. doi:10.1002/9780470141731.ch4

68. Chen W, Poirier B. Quantum Dynamical calculation of all rovibrational states of $HO_2$ for total angular momentum J = 0–10. *J Theor Comput Chem* (2010) 9:435–69. doi:10.1142/s0219633610005815

69. Huang S-W, Carrington T. A new iterative method for calculating energy levels and wave functions. *J Chem Phys* (2000) 112:8765–71. doi:10.1063/1.481492

70. Poirier B, Carrington T. Accelerating the calculation of energy levels and wave functions using an efficient preconditioner with the inexact spectral transform method. *J Chem Phys* (2001) 114:9254–64. doi:10.1063/1.1367396

71. Poirier B, Carrington T. A preconditioned inexact spectral transform method for calculating resonance energies and widths, as applied to HCO. *J Chem Phys* (2002) 116:1215–27. doi:10.1063/1.1428752

72. Poirier B, Miller WH. Optimized preconditioners for Green function evaluation in quantum reactive scattering calculations. *Chem Phys Lett* (1997) 265:77–83. doi:10.1016/s0009-2614(96)01408-x

73. Poirier B. Optimal separable bases and series expansions. *Phys Rev A (Coll Park)* (1997) 56:120–30. doi:10.1103/physreva.56.120

74. Poirier B. Quantum reactive scattering for three-body systems via optimized preconditioning, as applied to the O+HCl reaction. *J Chem Phys* (1998) 108:5216–24. doi:10.1063/1.475958

75. Poirier B. Efficient preconditioning scheme for block partitioned matrices with structured sparsity. *Numer Linear Algebra Appl* (2000) 7:715–26. doi:10.1002/1099-1506(200010/12)7:7/83.0.CO;2-R

76. Freund RW, Nachtigal NM. QMR: A quasi-minimal residual method for non-hermitian linear systems. *Numer Math* (1991) 60:315–39. doi:10.1007/bf01385726

77. Petty C, Chen W, Poirier B. Quantum Dynamical calculation of bound rovibrational states of $HO_2$ up to largest possible total angular momentum, $J \leq 130$. *J Phys Chem A* (2013) 117:7280–97. doi:10.1021/jp401154m

78. Petty C, Poirier B. Comparison of J-shifting models for rovibrational spectra as applied to the $HO_2$ molecule. *Chem Phys Lett* (2014) 605–606:16–21. doi:10.1016/j.cplett.2014.05.003

79. Yang B, Chen W, Poirier B. Rovibrational bound states of neon trimer: Quantum dynamical calculation of all eigenstate energy levels and wavefunctions. *J Chem Phys* (2011) 135:094306. doi:10.1063/1.3630922

80. Brandon D, Poirier B. Accurate calculations of bound rovibrational states for argon trimer. *J Chem Phys* (2014) 141:034302. doi:10.1063/1.4887459

81. Yang B, Poirier B. Quantum dynamical calculation of rovibrational bound states of $Ne_2Ar$. *J Phys B: Mol Opt Phys* (2012) 45:135102. doi:10.1088/0953-4075/45/13/135102

82. Yang B, Poirier B. Rovibrational bound states of the $Ar_2Ne$ complex. *J Theor Comput Chem* (2013) 12:1250107. doi:10.1142/s0219633612501076

83. Zhang Z, Li B, Shen Z, Ren Y, Bian W. Efficient quantum calculation of the vibrational states of acetylene. *Chem Phys* (2012) 400:1–7. doi:10.1016/j.chemphys.2012.01.010

84. Petty C, Spada RF, Machado FB, Poirier B. Accurate rovibrational energies of ozone isotopologues up to $J$= 10 utilizing artificial neural networks. *J Chem Phys* (2018) 149:024307. doi:10.1063/1.5036602

85. Sarka J, Poirier B. Comment on "Calculated vibrational states of ozone up to dissociation" [J. Chem. Phys. 144, 074302 (2016)]. *J Chem Phys* (2020) 152:177101. doi:10.1063/5.0002762

86. Sarka J, Petty C, Poirier B. Exact bound rovibrational spectra of the neon tetramer. *J Chem Phys* (2019) 151:174304. doi:10.1063/1.5125145

87. Sarka J, Poirier B. Hitting the trifecta: How to simultaneously push the limits of schrödinger solution with respect to system size, convergence accuracy, and number of computed states. *J Chem Theor Comput* (2021) 17:7732–44. doi:10.1021/acs.jctc.1c00824

88. Yurchenko SN, Thiel W, Jensen P. Theoretical ROVibrational energies (TROVE): A robust numerical approach to the calculation of rovibrational energies for polyatomic molecules. *J Mol Spectrosc* (2007) 245:126–40. doi:10.1016/j.jms.2007.07.009

89. Yurchenko SN, Yachmenev A, Ovsyannikov RI. Symmetry-adapted ro-vibrational basis functions for variational nuclear motion calculations: TROVE approach. *J Chem Theor Comput* (2017) 13:4368–81. doi:10.1021/acs.jctc.7b00506

90. Yurchenko SN, Mellor TM. Treating linear molecules in calculations of rotation-vibration spectra. *J Chem Phys* (2020) 153:154106. doi:10.1063/5.0019546

91. Czakó G, Furtenbacher T, Császár AG, Szalay V. Variational vibrational calculations using high-order anharmonic force fields. *Mol Phys* (2004) 102:2411. doi:10.1080/00268970420002749 91

92. Furtenbacher T, Czakó G, Sutcliffe BT, Császár AG, Szalay V. The methylene saga continues: Stretching fundamentals and zero-point energy of $X^3B_1$ $CH_2$. *J Mol Struct* (2006) 780–781:283–94. doi:10.1016/j.molstruc.2005.06.052

93. Mátyus E, Czakó G, Sutcliffe BT, Császár AG. Vibrational energy levels with arbitrary potentials using the Eckart-Watson Hamiltonians and the discrete variable representation. *J Chem Phys* (2007) 127:084102. doi:10.1063/1.2756518

94. Mátyus E, Šimunek J, Császár AG. On the variational computation of a large number of vibrational energy levels and wave functions for medium-sized molecules. *J Chem Phys* (2009) 131:074106. doi:10.1063/1.3187528

95. Fábri C, Mátyus E, Furtenbacher T, Mihály B, Zoltáni T, Nemes L, et al. Variational quantum mechanical and active database approaches to the rotational-vibrational spectroscopy of ketene, $H_2CCO$. *J Chem Phys* (2011) 135:094307. doi:10.1063/1.3625404

96. Mátyus E, Czakó G, Császár AG. Toward black-box-type full- and reduced-dimensional variational (ro)vibrational computations. *J Chem Phys* (2009) 130:134112. doi:10.1063/1.3076742

97. Fábri C, Mátyus E, Császár AG. Rotating full- and reduced-dimensional quantum chemical models of molecules. *J Chem Phys* (2011) 134:074105. doi:10.1063/1.3533950

98. Lauvergnat D, Nauts A. Exact numerical computation of a kinetic energy operator in curvilinear coordinates. *J Chem Phys* (2002) 116:8560. doi:10.1063/1.1469019

99. Lauvergnat D, Nauts A. Quantum dynamics with sparse grids: A combination of smolyak scheme and cubature. Application to methanol in full dimensionality. *Spectrochimica Acta A: Mol Biomol Spectrosc* (2014) 119:18–25. doi:10.1016/j.saa.2013.05.068

100. Nauts A, Lauvergnat D. Numerical on-the-fly implementation of the action of the kinetic energy operator on a vibrational wave function: Application to methanol. *Mol Phys* (2018) 116:3701–9. doi:10.1080/00268976.2018.1473652

101. Chen A, Nauts A, Lauvergnat D. *Elvibrot-mpi: Parallel quantum dynamics with smolyak algorithm for general molecular simulation* (2021). doi:10.48550/arXiv.2111.13655

102. Al-Refaie AF, Yurchenko SN, Tennyson J. GPU Accelerated intensities MPI (GAIN-MPI): A new method of computing Einstein-A coefficients. *Comput Phys Commun* (2017) 214:216. doi:10.1016/j.cpc.2017.01.013

103. Zhang JZH. *Theory and application of quantum molecular dynamics*. Singapore: World Scientific (1999).

104. T Pack R, Parker GA. Quantum reactive scattering in three dimensions using hyperspherical (APH) coordinates. Theory. *J Chem Phys* (1987) 87:3888–921. doi:10.1063/1.452944

105. Hougen JT. Classification of rotational energy levels for symmetric-top molecules. *J Chem Phys* (1962) 37:1433–41. doi:10.1063/1.1733301

106. Watson JKG. Simplification of the molecular vibration-rotation Hamiltonian. *Mol Phys* (1968) 15:479–90. doi:10.1080/00268976800101381

107. Watson JKG. Higher-order vibration-rotation energies of the $X_3$ molecule. *J Mol Spectrosc* (1984) 103:350–63. doi:10.1016/0022-2852(84)90062-6

108. Császár AG, Fábri C, Sarka J. Quasistructural molecules. *Wires Comput Mol Sci* (2020) 10:e1432. doi:10.1002/wcms.1432

109. Fábri C, Sarka J, Császár AG. Communication: Rigidity of the molecular ion $H_5^+$. *J Chem Phys* (2014) 140:051101. doi:10.1063/1.4864360

110. Asvany O, Yamada KMT, Brünken S, Potapov A, Schlemmer S. Experimental ground-state combination differences of $CH_5^+$. *Science* (2015) 347:1346–9. doi:10.1126/science.aaa3304

111. Fábri C, Quack M, Császár AG. On the use of nonrigid-molecular symmetry in nuclear motion computations employing a discrete variable representation: A case study of the bending energy levels of $CH_5^+$. *J Chem Phys* (2017) 147:134101. doi:10.1063/1.4990297

112. Fábri C, Császár AG. Vibrational quantum graphs and their application to the quantum dynamics of $CH_5^+$. *Phys Chem Chem Phys* (2018) 20:16913–7. doi:10.1039/c8cp03019g

113. Sarka J, Császár AG, Mátyus E. Rovibrational quantum dynamical computations for deuterated isotopologues of the methane–water dimer. *Phys Chem Chem Phys* (2017) 19:15335–45. doi:10.1039/c7cp02061a

114. Metz MP, Szalewicz K, Sarka J, Tóbiás R, Császár AG, Mátyus E. Molecular dimers of methane clathrates: *Ab initio* potential energy surfaces and variational vibrational states. *Phys Chem Chem Phys* (2019) 21:13504–25. doi:10.1039/c9cp00993k